Electrochimica Acta 222 (2016) 657–667

Contents lists available at ScienceDirect

Electrochimica Acta

journal homepage: www.elsevier.com/locate/electacta

Research paper

Self-assembled liquid crystalline nanotemplates and their incorporation in dye-sensitised solar cells

Muhammad Akmal Kamarudin[a,*], Ammar A. Khan[a], Calum Williams[a], Girish Rughoobur[b], Suhana Mohd. Said[c], Shabeena Nosheen[a], Andrew J. Flewitt[b], Malik M. Qasim[a], Timothy D. Wilkinson[a]

[a] Center of Molecular Materials for Photonics and Electronics (CMMPE), Department of Engineering, University of Cambridge, Cambridge, 9 JJ Thomson Avenue, CB3 0FA, United Kingdom
[b] Electronic Devices and Materials Group, Department of Engineering, University of Cambridge, Cambridge, 9 JJ Thomson Avenue, CB3 0FA, United Kingdom
[c] Liquid Crystal Display Laboratory, Department of Electrical Engineering, Faculty of Engineering, University of Malaya, 50603, Kuala Lumpur, Malaysia

ARTICLE INFO

Article history:
Received 7 September 2016
Received in revised form 31 October 2016
Accepted 5 November 2016
Available online 6 November 2016

Keywords:
Liquid crystals
reactive mesogen
self-assembled nanotemplate
polymer electrolyte
dye-sensitised solar cells

ABSTRACT

Liquid junction dye-sensitised solar cells (DSSCs) suffer from solvent evaporation and leakage which limit their large-scale production. Here, we have prepared DSSC using a simple and cheap fabrication process with improved photovoltaic parameters and stability. A binary mixture of Smectic A (SmA) and Nematic Liquid Crystal (NLC) was used to provide a self-assembled template for a polymerisable reactive mesogen LC. The layered structure of SmA combined with a low viscosity NLC forms a polygonal structure that provides an ordered and continuous template for reactive mesogens. Once the reactive mesogen is polymerised under UV light, the SmA:NLC mixture is washed away, resulting in a polymer network template containing nanochannels. We demonstrate the incorporation of these templates into DSSCs and find that DSSCs containing these nanochannels show improved open-circuit voltage (V_{OC}) (0.705 V) and short-circuit current (J_{SC}) (13.25 mA cm^{-2}) compared to that of the liquid electrolyte (V_{OC} = 0.694 V and J_{SC} = 10.46 mA cm^{-2}). The highest obtained power conversion efficiency with Sm-PE was 5.94% which is higher than that of the reference solar cell (5.51%). These can be attributed to the improved ionic conductivity and ionic diffusion of Sm-PE where the presence of the nanochannels aided the ionic conduction in the polymer electrolyte. In addition, it is hypothesized that the light scattering effect of the polymerised reactive mesogen also contributed to the improved performance of the photovoltaic devices. This finding is important because it is known fact that when a polymer is added to liquid electrolyte, the ionic conductivity will decrease although the stability is improved.

1. Introduction

Dye sensitised solar cells (DSSCs) were first demonstrated in 1991 by O'Reagan and Graetzel [1]. These hybrid organic-inorganic solar cells have the advantage of being environmentally friendly and also allow easy and low-cost fabrication without sacrificing their relatively high efficiency compared to organic solar cells. One of the major components of DSSCs is the electrolyte which is a redox mediator responsible for the regeneration of the dye and the electrolyte itself. The electrolyte in the DSSC device can be divided into three different types: liquid electrolyte, gel polymer electrolyte and solid state electrolyte. The liquid electrolyte DSSC gives the highest efficiency of up to 13% for Cobalt-based electrolyte [2]. However, this type of electrolyte suffers from evaporation of the solvent which reduces its long term stability. To address this issue, researchers have proposed the solid electrolyte which is more stable but sacrifices in the efficiency of the device as the solid electrolyte exhibits a low ionic conductivity. By employing various additives and plasticisers, it was found out that gel polymer electrolytes provide a compromise between solid and liquid electrolytes making it possible to extend the lifetime of the device without having to significantly sacrifice the efficiency [3–6]. On example of such an additive the addition of liquid crystalline (LC) materials to the electrolyte matrix [7,8].

LC materials exhibit physical properties that are intermediate between those of solids and liquids under certain conditions, *i.e.* temperature or solvent concentration. In addition, different molecular composition leads to the formation of different phases,

* Corresponding author. Tel: +44 (0) 1223 7 48365.
E-mail address: mak65@cam.ac.uk (M.A. Kamarudin).

http://dx.doi.org/10.1016/j.electacta.2016.11.021

such as nematic, smectic and columnar [9]. These characteristics come from intermolecular interactions as well as molecule geometry (cylinder or disc-like) which tends to self assemble in a given direction and sometimes in orientational order. Nematic phase is the simplest type of LC phase. Nematic phase shows thread-like discontinuities when observed under a crossed-polarised microscope. The thread-like discontinuities form what is called the Schlieren texture, where two or four dark brushes meet. The molecules tend to assemble with the long axes pointing toward a certain direction. Unlike nematic phase, smectic is much more viscous due the structure is much more closer to a solid where smectic phase not only has an orientational order but also a positional order. The molecules also tend to align in layers.

Despite their unique electro-optical properties that have allowed them to be used almost universally in display applications, LCs have had very limited use in photovoltaic applications. The exceptions to this has been work performed on the development of organic solar cells employing disc-like discotic liquid crystalline (DLCs) materials that have been shown to support higher charge carrier mobility than that of amorphous materials which is needed for a good electronic device [10,11]. A recent paper by Sun et al. shows that NLC could be use in organic solar cell with a high efficiency of 9.3% which is exceptionally high for an organic photovoltaic device [12]. LCs have also been shown to improve the efficiency of DSSC where the light scattering effect and the passivation of the TiO_2 surface by the LC material have been cited for this improvement [7,8].

Reactive mesogens (RMs) are a type of polymerisable LC material with a reactive unit at one or both ends of the molecule, with an acrylate being the most common end group. RMs undergo

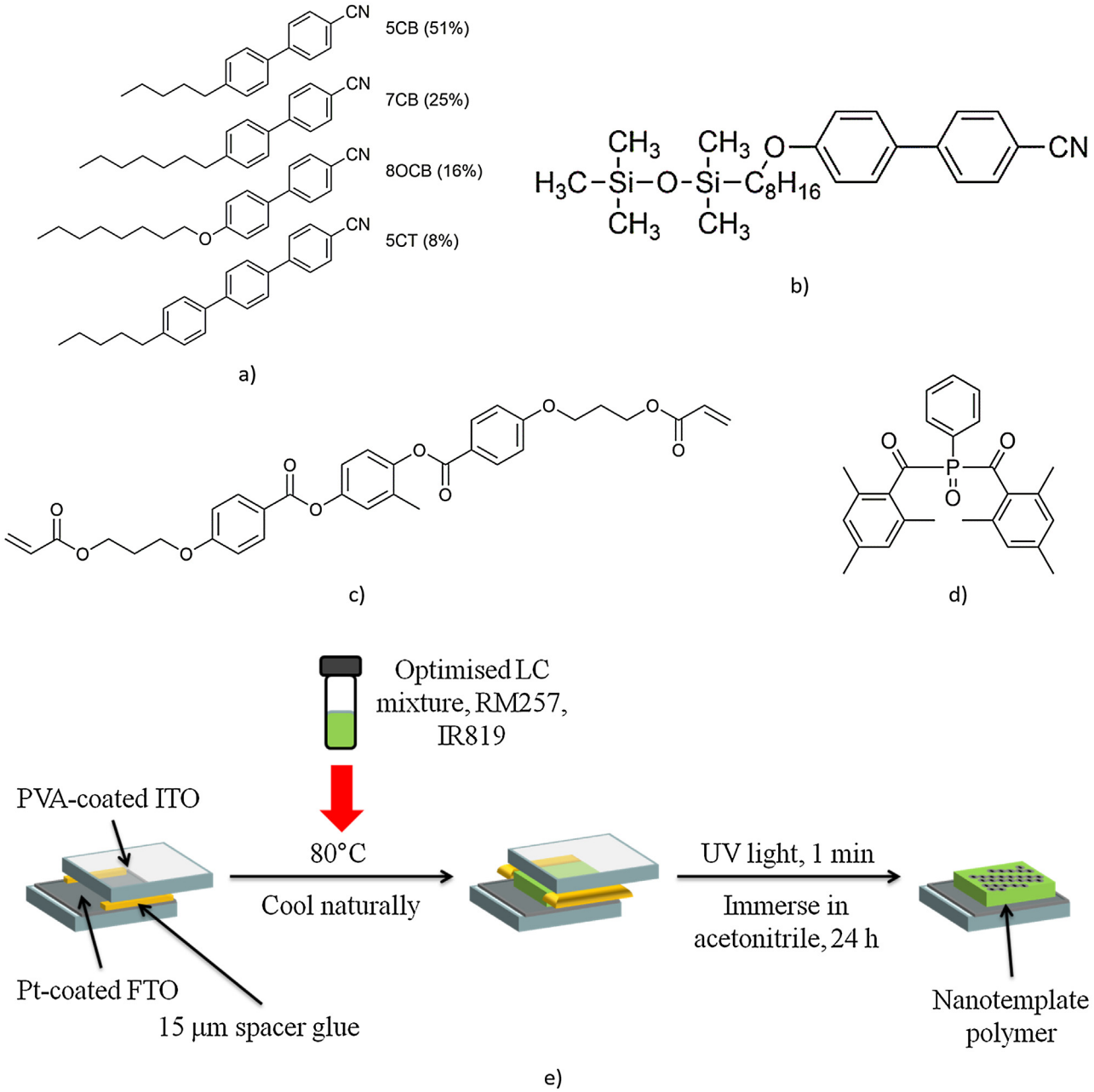

Fig. 1. Chemical structure of a) nematic E7, b) smectic 8/2 organosiloxane, c) the reactive mesogen, RM257, d) the photoinitiator, IR819 and e) schematic illustration of nanotemplate preparation.

polymerisation in the presence of photoinitiator and UV light. Even after polymerisation, RM still retain their anisotropic properties which makes them interesting materials for a range of applications such as displays and organic light emitting diodes (OLEDs) [13,14].

In DSSC research, the use of nanostructures has been employed to further increase the efficiency by enhancing the semiconductor material's charge transport properties. Most of these experiments however, investigate the effect of nanostructured growth in the transparent oxide semiconductor by using ZnO, and TiO_2 *etc.* [15,16]. Lim et al. have shown that the templating technique can be used to prepare oxide semiconductors where block-graft copolymers were employed to prepare a highly organised TiO_2 mesoporous layer [17]. This approach has given the rise to the concept of utilising nanostructures with the redox electrolyte to improve the ionic conduction mechanism. This concept has been explored by Horgberg et al. who used a binary LC mixture to form nano-segregated structures for DSSCs, which are able to perform well up to 120 °C [18].

In this study, we propose a new type of electrolyte, through the use of highly ordered Smectic A (SmA)/NLC mixture which provides a template for the assembly and alignment of RM components. The RM is responsible for making a polymer network when exposed under UV light. Templating techniques have been successful in providing a highly ordered self-assembled structure in the polymer electrolyte systems, which in turn, improved the carrier mobility and conductivity of the templated material [19–21]. To define the role of SmA and NLC in the formation of the self-assembled nanotemplate interaction, a series of binary mixtures with different SmA:NLC ratio were prepared and characterised through polarising optical microscopy (POM). The optimised binary LC mixture was used to fabricate DSSC and the photovoltaic properties are characterised.

2. Experimental

2.1. Materials

E7 LC was received from Merck. Lithium iodide (LiI), Iodine (I_2) and 4-tert-butylpyridine (TBP) were purchased from Sigma-Aldrich. Ti-Nanoxide D/SP Paste, 1,2-dimethyl-3-propylimidazolium iodide (DMPII) and meltonix 1170-25 (DuPont Surlyn®) were purchased from Solaronix. Di-tetrabutylammonium cis-bis(isothiocyanato)bis(2,2′-bipyridyl-4,4′-dicarboxylato)ruthenium(II) (N719) dye was received from Organica®. RM257 and IR819 were obtained from Merck. All materials were used as received without further purification. 8/2 organosiloxane has been synthesised in house according to previous work [22].

2.2. Liquid crystal binary mixture preparation

LC mixtures of SmA (8/2 organosiloxane) and NLC (E7) were prepared with respect to different ratios. The binary LC mixtures were mixed together by placing them in an oven and bringing them above their isotropic temperatures (80 °C) for 4 hours to obtain a homogenous mixture. The resulting mixtures were used for further characterisations. The structures of the materials are shown in Fig. 1. Table 1 shows the different ratios of the LC components to prepare the LC mixtures.

Table 1
Summary of the SmA:E7 binary LC mixtures.

Mixture	1	2	3	4	5
SmA	0	20	40	60	100
E7	100	80	60	40	0

2.3. Liquid crystal nanostructure-template preparation

The optimised binary LC mixture was then mixed with a reactive mesogen (RM257) and a photoinitiator (IR819). The RM molecule has two acrylate functional groups which can undergo polymerisation under the presence of UV light. The mixture was heated in an oven above the isotropic temperature for 4 hours. After that, the mixture was filled into a cell with a thickness of 15 um and cured using a UV light (1 mW/cm2) for 1 min. The cell was fabricated with platinum-coated fluorine-doped tin oxide (FTO) substrate on one side and polyvinyl alcohol (PVA)-coated glass substrate on the other side. The FTO substrates were spin-coated with platinum paste (Dyesol's PT1 Platinum Paste) at 2000 r.p.m for 60 s and annealed at 450 °C for 30 mins. The PVA layer on the other substrate acts as a sacrificial layer so that it is easy to crack open the cell afterwards. Once the mixture has been polymerised, the LC component was removed by immersing the cell in acetone for 24 hours. The cell was then cracked open leaving the nanochannel template on the platinum side. The substrate was then used to fabricate DSSC. Fig. 1 shows the chemical structures of the materials used and the schematic diagram of preparing nanotemplate polymer.

2.4. Device fabrication

The photoanodes were prepared by spin-coating a thin layer (100 nm) of compact TiO_2 onto FTO substrate and annealed at 450 °C for 30 mins. The spin-coated substrates were then bar-coated with titania paste (Dyesol's 18NR-T Transparent Titania Paste) and then annealed at 500 °C for 30 mins. The resulting thickness was approximately 8 μm. The substrates were then immersed in 0.3 mM N719 dye solution for 24 hours. Excess dye was removed by washing the substrate with acetonitrile for several times. The photoanode and the photocathode with nanochannel template were glued together using 25 μm sealing film (Meltonix 1170-25). The electrolyte which consists of 0.6 M MPII, 0.5 LiI, 0.05 I_2 and 0.5 M TBP in acetonitrile were capillary filled into the cell. The active area of the cell is controlled to be 0.283 cm^2.

2.5. Characterisations

The Differential scanning calorimetry (DSC) was employed to determine the transition temperature of the LC. The measurement was performed using a Mettler Toledo DSC 823e at a heating and cooling rate of 5° C min^{-1} from 0° C to 100° C. An Olympus polarising optical microscope (BX60) attached to a programmable hot-stage was used to obtain the morphology of the LC mixtures. The samples were brought to isotropic and slowly cooled down to their liquid crystal phase. All images were taken at their respective liquid crystal temperature. The heating or cooling temperature was controlled at 5° C min^{-1}. In the case of the templated polymer, POM images were taken at room temperature. The Fourier transformed infra-red (FTIR) spectroscopy was performed on silicon substrate in transmission mode from 4000 to 1400 cm^{-1} using PerkinElmer. The ex situ characterisation of the polymer on silicon substrate was carried out using scanning electron microscopy (SEM, Zeiss SigmaVP, 2 kV). The conductivity measurement was performed using a Keithley 4200-SCS parameter analyzer. The measurement was performed at room temperature in a ITO-ITO cell with 25 μm thickness. The light scattering effect of the sample was investigated using a red LED diode laser (650 nm) with an elliptical beam. The sample was placed 10 cm from the laser and a beam stop was used to remove the zero-order of the output light so that the scattered light can be observed more clearly. *J-V* measurement of the solar devices was performed using Keithley sourcemeter connected to the Labview

program developed in-house. The measurement was performed from −1.0 to 1.0 V at 100 mW/cm^2 sunlight at AM 1.5G (1 sun). Electrochemical Impedance spectroscopy (EIS) and steady state voltammogram were performed on a Solatron 1260 Impedance Analyzer. For the EIS, the measurements were carried out in the frequency range of 10 mHz to 1 MHz with a 10 mV step under dark. For the steady-state voltammogram, the measurement was carried out from −1.5 V to 1.5 V at a rate of 10 mV s^{-1}.

3. Results and discussion

Binary mixtures of 8/2 organosiloxane and E7 were prepared with varying weight percent (wt.%). Fig. 2a shows the DSC curves of binary LC mixtures of a nematic (N) E7 and a 8/2 organosiloxane LC. The transition temperature for pure E7 from N to isotropic (I) is 58.3 °C. The 8/2 organosiloxane showed a SmA phase within the temperature range of 43.6 °C to 62.9 °C, and is crystalline at room

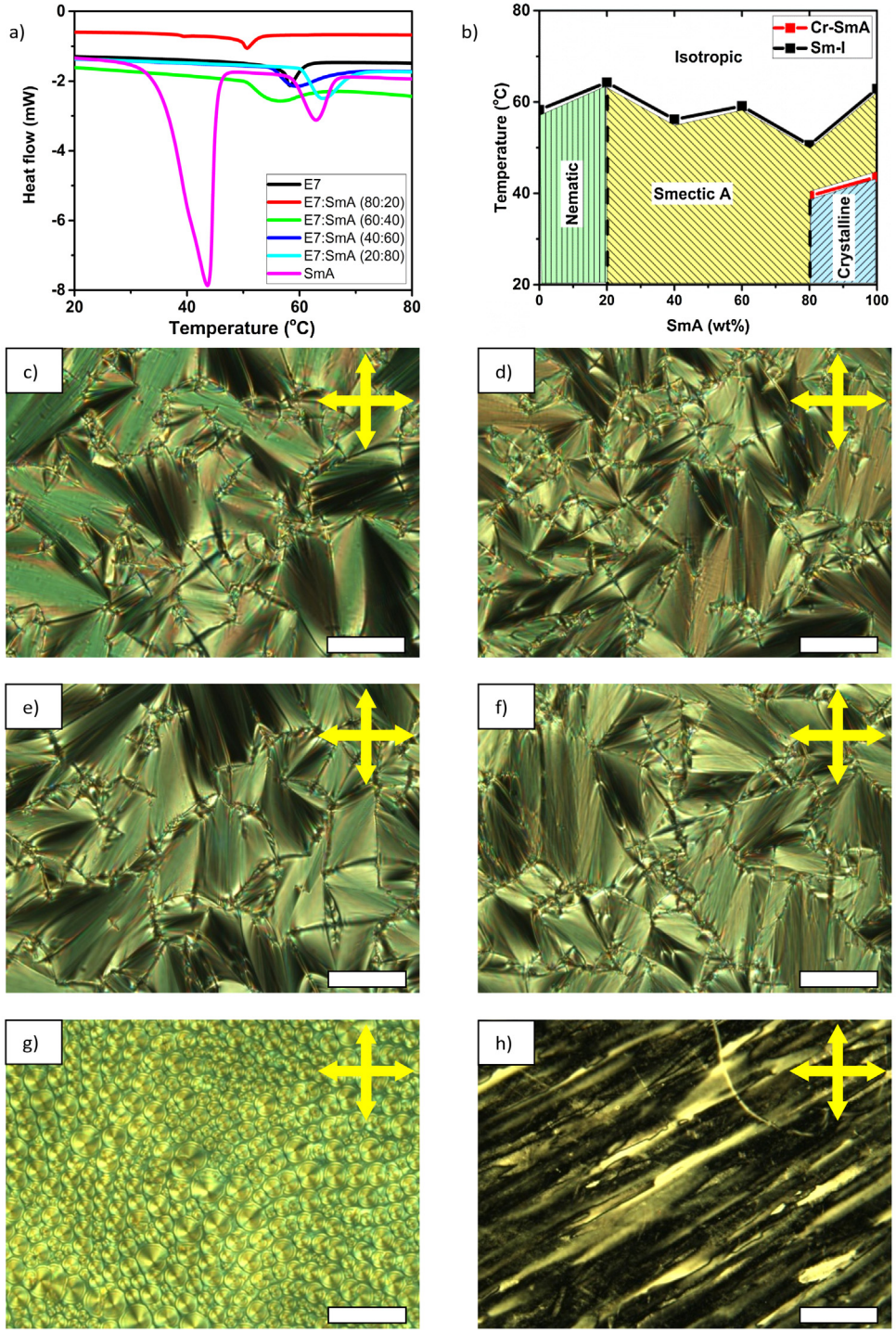

Fig. 2. a) DSC curves under heating at 5 °C/min and b) phase diagram of pure LC materials and binary liquid crystal mixtures at different 8/2:E7 ratio. POM micrographs of LC mixture at different 8/2:E7 ratio under crossed polarisers. All pictures are taken at their LC phase after cooling down from isotropic at a rate of 5 °C/min. c) 100:0, d) 80:20, e) 60:40, f) 40:60, g) 20: 80 and h) 0:100. The scale bar is 50 μm.

temperature in its native form. The addition of 20 wt.% of 8/2 organosiloxane to E7 increased the SmA to I transition temperature up to 64.3 °C which is the highest obtained transition temperature for pure materials and binary mixtures. A further increase in the E7, however resulted in a lower transition temperature. The lowest transition temperature was displayed by the 8/2:E7 20:80 mixture at 50.6 °C. From the DSC study, it is evident that the mixtures are homogenous, as the transition temperature of the pure materials were not observed within the DSC plots of the mixtures.

In order to get a clearer picture of the LC phases as a function of the composition of the binary LC mixtures, its phase diagram is plotted (Fig. 2b). The measurement of the transition temperature is limited by the DSC equipment and the measurement below 0 °C could not be obtained. The addition of 8/2 organosiloxane to E7 drastically changed the mesophase where only the smectic phase could be obtained. The mesophase is thought to be dependent on the larger size of the LC component and in this case, the phase of the binary mixture is induced by the 8/2 organosiloxane where the size of the molecule is a few times larger than E7. The effect of the LC length on the mesophase of a binary LC mixture has been studied previously [23]. For 8/2:E7 20:80 mixture, not only the transition temperature is the highest, but it also has a wider SmA temperature range compared to the pure 8/2 organosiloxane and other binary mixtures.

Fig. 2 also shows the morphology of the LC mixtures in their LC phase as observed using the POM. SmA phase is characterised by the fan-shaped structure which are made up of focal conics (Fig. 2c). This is formed from lamellae structure where the smectic layers are parallel to the substrate's plane. On the other hand, E7 showed a Schlieren texture which is typical for NLC (Fig. 2h). In the

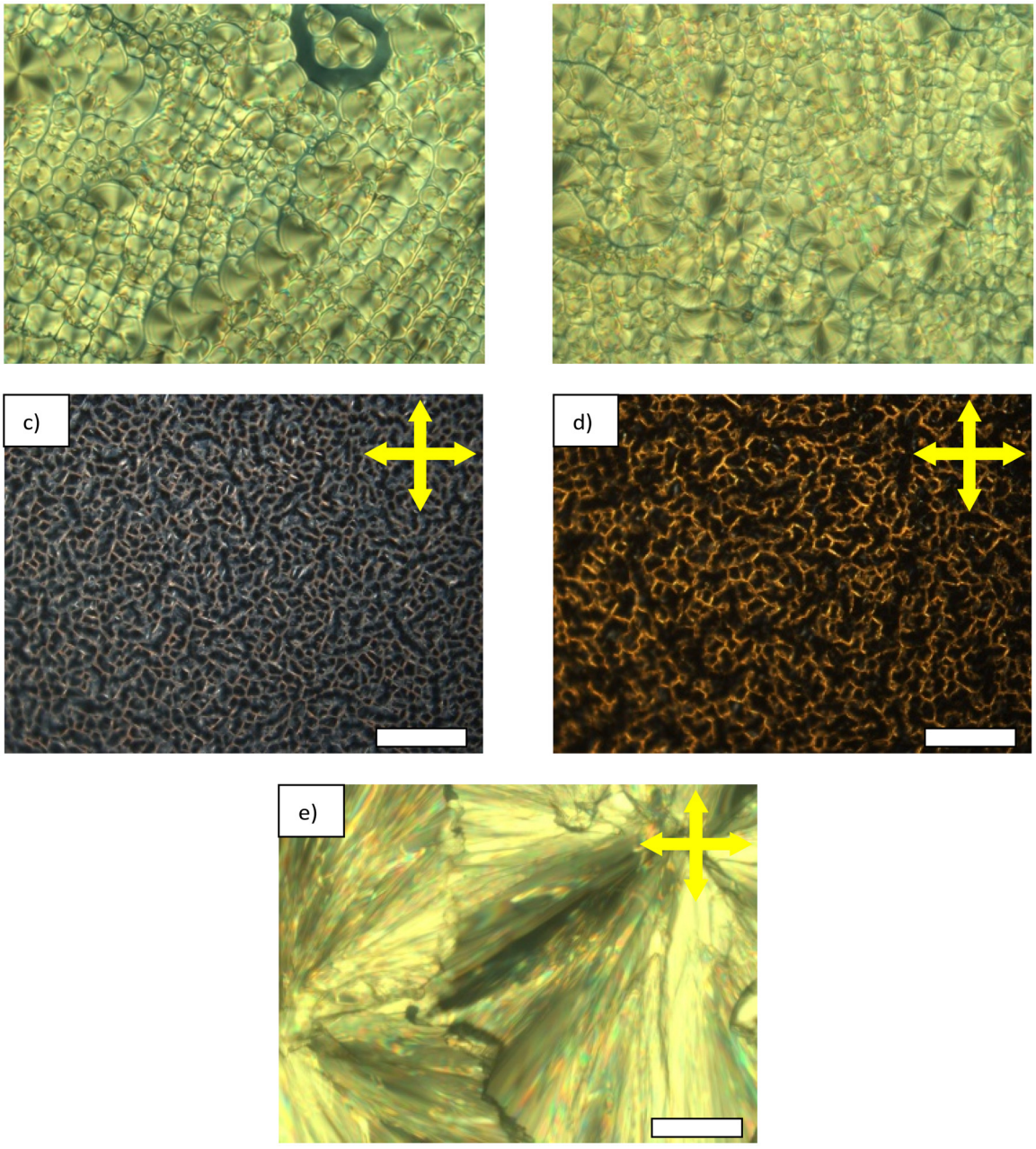

Fig. 3. POM micrographs of SmA:E7 mixture with RM 257 and IR819 under crossed polarizers observed at room temperature. The cell is filled in the isotropic state and is allowed to cool down naturally before characterisation. a) Before polymerisation, b) after polymerisation, c) after removal of LC, d) after infiltration with liquid electrolyte, and e) pure RM257. The scale bar is 50 μm.

8/2:E7 20:80 mixture, a polygonal structure could be seen (Fig. 2g). This is a result of disclination of the lamellae perpendicular to the plane of the glass substrates which induces the focal ellipses lying in the plane. The tip of the focal section affixed to the opposite substrates. This type of texture can only be seen in 8/2:E7 20:80 mixture. Beyond 20 wt.% concentration of 8/2 organosiloxane, all of the mixtures showed the typical SmA texture as can be seen from Fig. 2d–f. It is found out that the optimum ratio of 8/2 organosiloxane to E7 is 20:80 as this mixture gives a structure that is standing up instead of lying on the plane of the substrate and thus a higher degree of order. This result is also supported by the DSC thermogram where 8/2:E7 20:80 showed the highest transition temperature among other mixtures. Hence this mixture is chosen to be used as the template for the electrolyte to be used in DSSC fabrication.

In order to form stabilised nano-templates, a polymerisation step is required. This was achieved through the addition of LC monomer RM257 to the original binary mixtures. The binary LC mixture acts as a template upon which RM257 will assume the morphology or texture induced by the binary mixture. No change in the texture of the mixture was observed after the addition of RM257 and IR819 showing the stability of the polygonal structure. The morphology of the mixture before (Fig. 3a) and after polymerisation (Fig. 3b) were the same showing that the polymerisation did not change the morphology of the optimised mixture. The RM257 has been successfully templated using the binary mixture as seen from Fig. 3a and b instead of showing the spherulite structure of RM257 (Fig. 3e). The LC component was then removed using acetone to leave polymerised nano-channels (Fig. 3c). After removal of the LC constituents, the textures showed hollow inter-connected channels. This shows that the RM has been templated using the binary LC mixture where the RM filled the space between the micro-platelets of the polygonal structure. It is postulated that the iodide based liquid electrolyte ions travel through these nano-channels. Filling the cell with the liquid electrolyte (Fig. 3d) preserves the same structure which means that the template is stable with regards to acetonitrile. The image of the electrolyte within the smectic-templated polymer electrolyte (Sm-PE) is indicated in yellow due to the presence of the iodine in the electrolyte.

FTIR spectroscopy was performed for different materials to study the interaction between different molecules and the changes after UV polymerisation. The absorption corresponding to the nitrile group is around 2200 cm^{-1} which is present in E7, 8/2 organosiloxane and the binary LC mixtures. Fig. 4 shows the FTIR curves for the different pure materials and mixtures. After the removal of the LC components, it can be clearly seen that this peak has disappeared, showing that acetone has removed the LC and leaving only polymerised RM257. The peak at 1700 cm^{-1} originates shows the C=O stretching coming from RM257. This peak still exists even after immersing the sample in acetone which proves that acetone only removed the LC components. Fig. 4 shows the FTIR spectra for the LC material, the mixture before and after UV polymerisation and also after immersion in acetone.

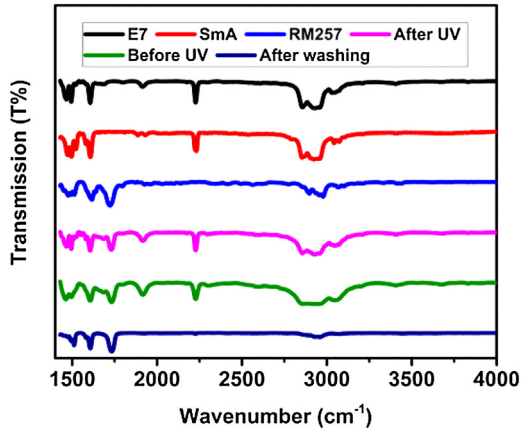

Fig. 4. FTIR spectra of the different components of the pure E7, 8/2 organosiloxane, RM257, the binary mixtures before and after UV curing and after the removal of the LC components.

Fig. 4. FTIR spectra of the different components of the pure E7, 8/2 organosiloxane, RM257, the binary mixtures before and after UV curing and after the removal of the LC components.

SEM micrograph allows for a more precise view of the polymerised mixture after removal of LC components (Fig. 5a). As can be seen from the micrograph, nano-sized pores formation could be observed throughout the sample. These hollow structures are postulated to be provide ordered pathways for mobile ions to move, and at the same time have the ability to trap liquid electrolyte and thus extend the lifetime of the polymer electrolyte by suppressing the evaporation of the solvent. The width of the polymer fibre is estimated to be around 50 nm. The polymer has a thread-like structure where two or more polymer fibres intertwine. It is also found that the surface roughness is considerably high. This is to be expected as the UV polymerisation of the sample was performed in a cell. The process of removing the top and bottom substrates might have led to the uneven surface despite the use of PVA as the sacrificial layer. Another thing to note is the formation of bigger thread-like structure formed by different single polymer fibres. These intertwined thread-like structures form boundaries resulting in the configuration of the micron-sized pores as seen in the POM micrographs. AFM studies have also been performed on the same sample. The AFM micrograph (Fig. 5b) corresponds well with the SEM image where the formation of helical structures could be seen. The width of the polymer is also estimated to be around 50 nm which is in good agreement with the SEM image. In addition it can be seen that the surface of the template is not smooth, but in fact displays surface variations of about 1 μm.

Fig. 5 (a) SEM image of LC-templated polymer with a thin layer of chromium/gold sputtered onto the sample to reduce the charge build-up during characterisation. (b) AFM image of the LC-templated polymer prepared on silicon substrate.

Ionic diffusion constant of the mobile ions in the template electrolyte was measured using a standard current density limited method using the steady-state voltammogram. The diffusion coefficient can be calculated using the following equation (Eq. (1))

$$J_{\lim} = \frac{2nFD_{I_3^-}c_{I_3^-}}{l} \quad (1)$$

where n is the electron number per molecule, F is the Faraday constant, $D_{I_3^-}$ is the diffusion coefficient of the limiting compound, and $c_{I_3^-}$ is the initial concentration of the limiting compound [24]. From the measurement, it was calculated that the $D_{I_3^-}$ of liquid electrolyte is 2.59×10^{-6} cm s^{-1} and the Sm-PE showed $D_{I_3^-}$ of 4.53×10^{-6} cm s^{-1}. The increased of $D_{I_3^-}$ in the case of Sm-PE can be related to the improved motion of the ions in the highly ordered nanostructure which provided a more efficient pathway for the movement of the mobile ions instead of moving randomly. The presence of polymer network can also be thought of as a barrier for the mobile ions to recombine with each other to form a tightly bound compound which effectively reduce the ion diffusion. Fig. 6 shows the steady-state voltammetry measurement for different electrolytes.

Current-voltage measurement was performed to measure the ionic conductivity were performed at room temperature. The ionic

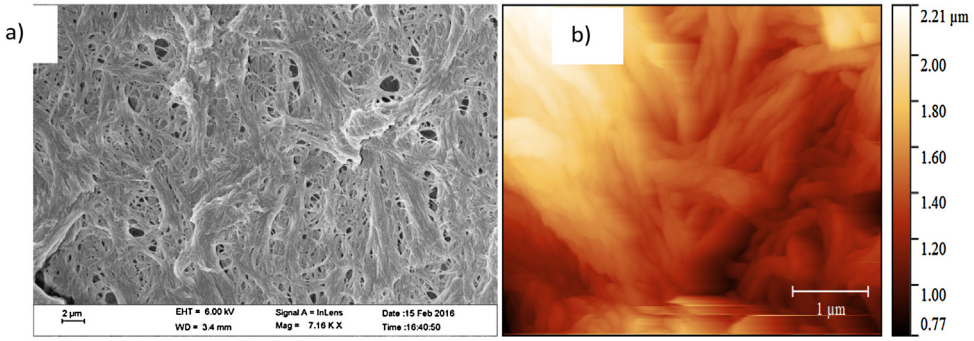

Fig. 5. a) SEM image of LC-templated polymer with a thin layer of chromium/gold sputtered onto the sample to reduce the charge build-up during characterisation. b) AFM image of the LC-templated polymer prepared on silicon substrate.

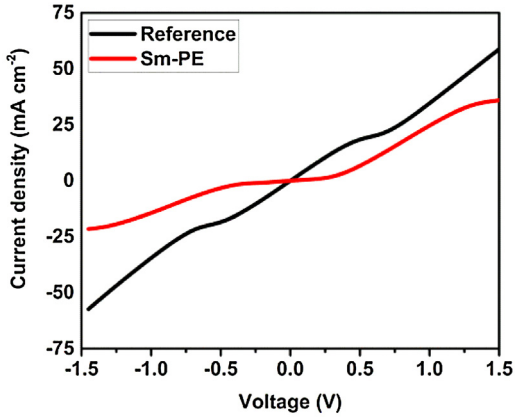

Fig. 6. Steady-state voltammetry curve of the reference electrolyte and Sm-PE performed at room temperature in a 25 µm cell.

conductivity of the templated Sm-PE is significantly higher than that of the reference electrolyte by almost 2-fold, from 7.70×10^{-4} S m^{-1} for the reference electrolyte and 1.47×10^{-3} S m^{-1} for the Sm-PE. It has been shown that the ionic conduction mechanism in polyethylene oxide is through the coordination process of lithium ions induced by the segmental motion of the polymer backbone. The ions either as singular or clusters move along the same chain or different chain through hopping mechanism due to the formation and breaking of the Li-O bonds present in the polymer [25]. This clearly strengthens the assumption that the channels help to increase the ionic conduction through a more ordered ionic hopping process as the polymer itself is an insulator and does not contribute to electronic conduction. Similar observations were also noted by Majewski et al. who measured higher ionic conductivity in the case of liquid crystalline polymer electrolyte structure prepared perpendicular to the two electrodes [26]. Since the ion transport mechanism in the polymer electrolyte involves the percolation of the mobile ions between boundary zones, a mesoporous insulating network will force the particles to touch or come close to each other so as their space-charge zones overlap [27]. This enhances the space-charge effect and hence the ionic conductivity. Table 2 summarises the ionic conductivity and ionic diffusion for different electrolytes.

Table 2
Ionic conductivity data for reference liquid electrolyte and electrolyte prepared by UV-polymerisation of the LC mixture.

Sample	Ionic diffusion (cm s^{-1})	Ionic conductivity (S m^{-1})
Liquid electrolyte	2.59×10^{-6}	7.70×10^{-4}
Sm-PE	4.53×10^{-6}	1.47×10^{-3}

The function of the reactive mesogen here is to act as the polymer matrix and this is the first report that showed the use of RM257 in DSSC application. RM257 is a known insulator and thus has an extremely low conductivity compared to the liquid electrolyte. The application of RM257has long been limited to display technology. In this case, RM257 was used to prepare the polymer matrix and the binary LC mixture acts as the template for the polymerisation process. The function of this polymer matrix is to contain and aid the conduction of the liquid electrolyte. The polymer itself is not involved in the electrochemical reaction of the liquid electrolyte. It is reasonable to assume that the ionic conduction occurring in the Sm-PE is the same as any other polymer electrolyte in which the segmental motion of the polymer backbones together with inter- and intra-chain ionic hopping. The redox reaction in this case remains the same as that of a standard electrolyte used:

$$\frac{1}{2}I_3^- + e_{(Pt)} \rightarrow \frac{3}{2}I^-$$

$$I_3^- + 2e_{(Pt)} \rightarrow 3I^-$$

Light propagation in a solar cell is an important factor that can affect the efficiency of solar devices [28], and increasing the effective propagation length of light in a solar cell serves to increase device efficiency by enhancing optical absorption by the active medium. A light scattering experiment was performed on the two samples to investigate how light scattering varies with and without the Sm template. Fig. 7 shows a schematic of the light scattering setup utilised to compare the two samples. A 650 nm laser diode with an elliptically-shaped output beam was incident onto the sample and the scattering profile was observed in the farfield (Fig. 7a). As can be seen from the pictures, the light profile for the cell before (Fig. 7b) and after filling (Fig. 7c) with liquid electrolyte is similar, implying that there no significant increase in light scattering on filling optically isotropic liquid electrolyte. However, a significant increase in scattering could be seen for the un-filled cell employing the Smectic-templated polymer (Fig. 7d) due to the incorporation of a birefringent porous medium inside the beam path. On filling a liquid electrolyte into the templated polymer the beam spread/scattering is reduced (Fig. 7e). This is due to better refractive index matching between the liquid electrolyte and the polymer template [29]. Increasing the light scattering within the solar cell effectively increases the probability of the light of exciting the dye molecules and hence increase the J_{SC} [30,31].

Subsequently, DSSCs were fabricated using the stabilised nanochannel-templated electrolyte, and tested under AM 1.5

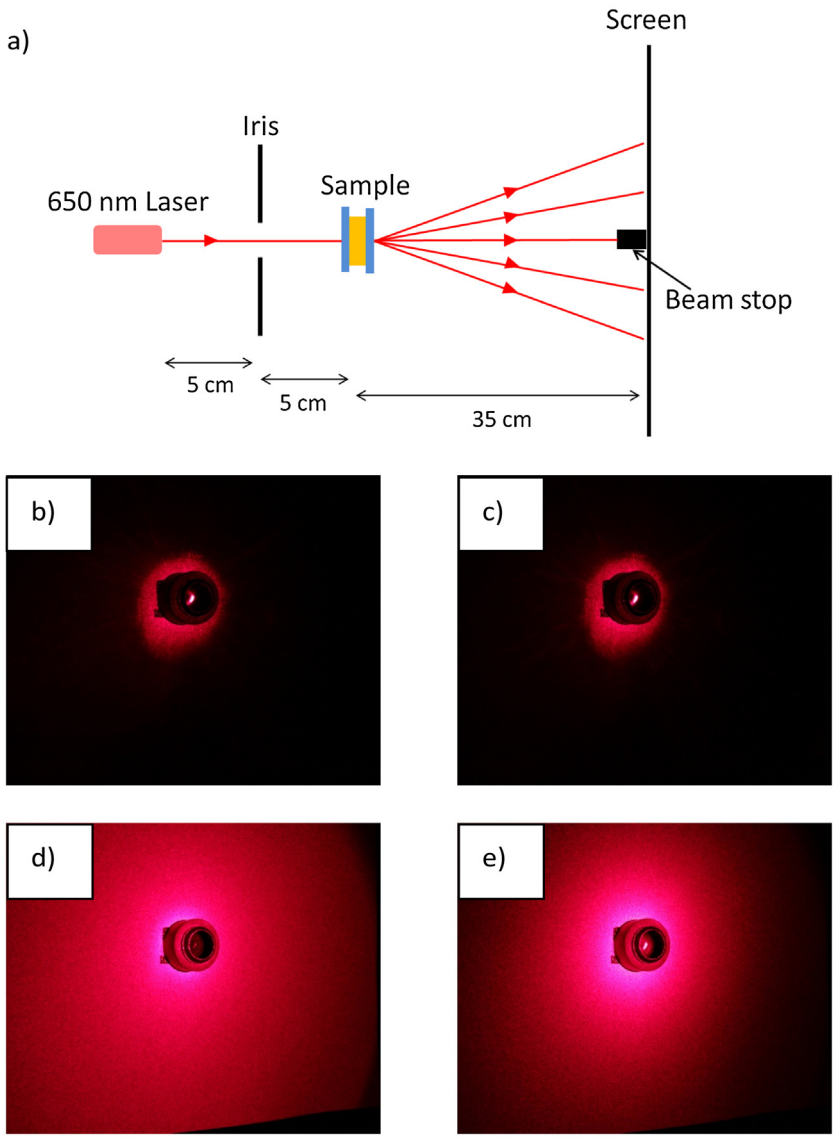

Fig. 7. a) Schematic diagram for the light scattering experimental setup and the output profile of b) empty cell, c) cell filled with liquid electrolyte, d) empty cell containing Smectic-templated polymer and e) cell containing Sm-PE. The ITO-ITO cell were fabricated using 25 μm spacer film.

conditions. The *J-V* curves and a summary of the efficiencies of the solar cells are shown in Fig. 8 and Table 3 respectively. For comparison, a DSSC employing standard liquid electrolyte was measured in addition to the Sm-PE sample. The liquid electrolyte shows a V_{OC} = 0.694 V, a J_{SC} = 10.46 mA cm^{-2} and a FF = 68%, corresponding to an efficiency, η of 5.51%. The device which has been polymerised on the counter electrode side exhibits a V_{OC} = 0.705 V, a J_{SC} = 13.25 mA cm^{-2} and a FF = 63%, corresponding to η of 5.94%.

In particular, the improvement in J_{SC} of 11% was achieved for the Sm-PE which can be attributed to a more ordered ionic conduction pathways which enhance the ionic transport within the polymer. This is evident from the ionic conductivity data where the Sm-PE showed higher ionic conductivity. This might seem initially counterintuitive as the nonconductive polymer covering much of the surface of the platinum and thus reduces the area of catalytic reaction of platinum and triiodide and yet still gives a higher photocurrent. In the other case of polymer electrolyte, the J_{SC} is lowered due to the movement of mobile ions hindered by the polymer network but this is not the case in polymer template electrolyte [32]. This supports our hyphothesis that the ionic conduction is aided by these nanopores in the case of the LC-templated electrolyte. The DSSC fabricated with Sm-PE also showed an increase in the V_{OC}. This reduction in the FF is attributed to the increase in the series resistance within the device.

Fig. 8 shows the *J-V* characteristics of the two different types of solar devices under (a) light (b) dark conditions. The dark current gives the information on the kinetics of the reaction of the electrons from mesoporous TiO_2 with triiodide in the electrolyte. The liquid electrolyte showed an onset of dark current which is a few mV lower than that of Sm-PE. This shows that the liquid electrolyte has larger recombination than Sm-PE. The curve also showed an increase in the photocurrent with the increase in the voltage, suggesting the suppression of the recombination reaction with the use of the Sm-PE.

EIS measurement was performed to investigate the charge transport mechanism in the devices [33–35]. Fig. 8(c) shows the Nyquist and (d) bode plot of the devices measured under dark at an applied bias of −0.7 V. The equivalent circuit for the EIS measurement given by Fig. 8e as has been used in previous literatures [36,37]. The resistances and the electron lifetime are summarised in Table 4. The series resistance is a major parasitic

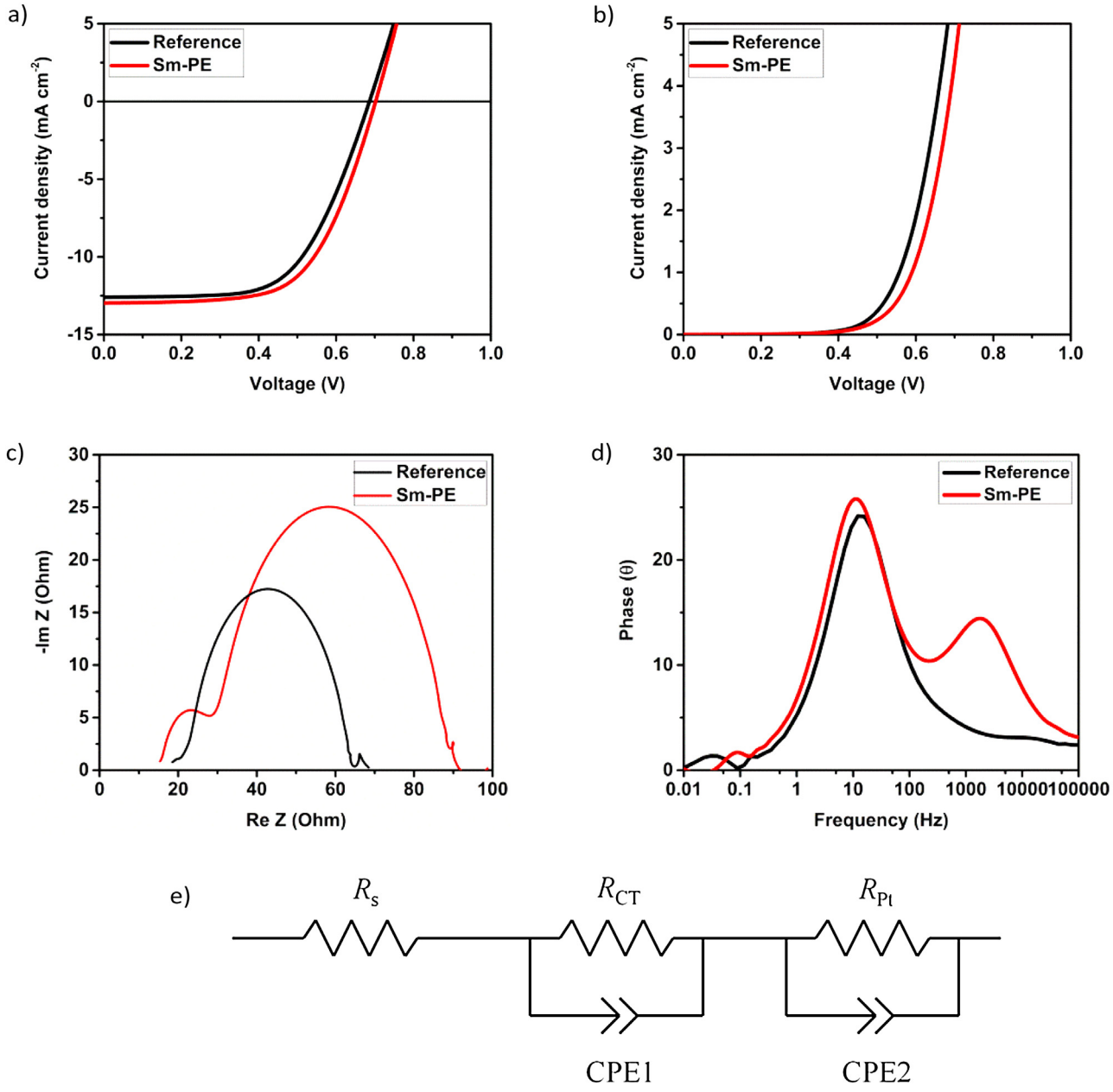

Fig. 8. *J-V* curves of DSSC with reference liquid electrolyte and Sm-PE electrolyte under a) dark and b) light. c) Nyquist and d) bode plot of DSSCs under dark condition at −0.7 V applied bias. e) The equivalent circuit used to determine resistances in the solar device. The measurements were performed at room temperature.

Table 3
Photovoltaic performance of DSSCs based on reference liquid electrolyte and Smectic-templated polymer electrolyte. The value in the bracket shows the value for the champion cell.

Device	J_{SC} (mA cm^{-2})	V_{OC} (V)	FF (%)	η (%)
Reference	10.69 (10.46)	0.696 (0.694)	64 (68)	4.81 (4.97)
Sm-PE	11.92 (13.25)	0.699 (0.705)	64 (63)	5.29 (5.94)

Table 4
Summary of EIS parameters for liquid electrolyte and Sm-PE DSSCs.

Device	R_s (Ω)	R_{ct} (Ω)	τ_n (ms)
Reference	18.53	42.74	11.43
Sm-PE	15.07	63.63	14.33

resistance that significantly affects the performance of a solar cell. The series resistance originated from the different charge transfer process at the Pt electrode, charge carrier transport in the electrolyte and the sheet resistance of the FTO substrate. From the Nyquist plot above, the sheet resistance, R_s of the platinum electrode can be extracted. The R_s is smaller in the case of Sm-PE, largely due to improved charge carrier transport which has been explained previously. The charge transfer resistance at the TiO_2/dye/electrolyte interface is given by the R_{ct} which can be determined from the diameter of the second semicircle. The R_{ct} is lower in the case of reference DSSC compared to Sm-PE which means that the excited electrons are easily injected into the TiO_2. The formation of nanostructures in the case of Sm-PE impede the movement of the electron within the device and thus lowers the charge transfer rate. This observation agrees with the finding obtained in the ionic diffusion experiment.

The electron lifetime can be calculated from the Bode plot using the following equation

$$\tau_n = \frac{1}{2\pi f_{max}}$$

where f_{max} is the frequency of the peak in the medium frequency [38]. The electron lifetime is related to the back reaction between the injected electron from the dye and the recombination reaction with the electrolyte instead of being transported into the system. It has been shown that the use of a thin TiO_2 compact layer can help to reduce this back recombination reaction and improve the electron lifetime [39]. In this experiment, the Sm-PE showed an improved electron lifetime compared to the reference liquid electrolyte DSSC which suggest that the back reaction has been impeded by the insulating polymer template. The channels can be thought of as a barrier which prevent the injected electrons in the TiO_2 from being intercepted by the mobile ions in the redox electrolyte.

4. Conclusions

Binary mixtures of varying compositions of the SmA and N are prepared and characterised, and the mixture showing the most ordered textures under crossed polarisers is identified. It is shown that the structure of the phases depends strongly on the SmA component because the molecule is larger compared to E7. The function of this binary LC mixture is to provide a template for the RM LC which will be added later. The RM is then added to the optimised binary LC mixture and UV-polymerised to form highly ordered, self-assembled RM polymer network. As a potential application of the LC polymer templates, we prepare DSSC devices. DSSCs fabricated using these nanostructures show promising properties such as an increase in the V_{OC}, J_{SC} and η. The increase in the photovoltaic parameters is thought to be due to the formation of channels that aided the ionic conduction and the increased in the electron lifetime which has been supported by the EIS measurement. Further to this, the light scattering by the Sm-PE also plays a role in increasing the efficiency as it increases the probability of the dye being excited by the incoming light. Further improvement could be attained by using different reactive mesogen which can respond well with the ionic liquid component which has been used in this study. Further development of these templated electrolytes has the potential of enhancing the PCE even further. The self assembly of nanochannels for containment of electrolyte to form polymer electrolyte can be exploited in a number of energy storage/conversion applications. These results demonstrate a new pathway on the possibility of incorporating LCs to provide an ordered template into DSSC research and widen the possibility and application of these self-assembled nanostructure in the field of photovoltaic research and could include applications in Li-ion batteries, fuel cells, capacitors and solar cells.

Acknowledgements

The authors would like to thank Organica and Dyesol for providing the materials used in this experiment. A.A.K. and G.R. would like to thank the Cambridge Commonwealth Trust for financial support. A.A.K. would also like to thank the HEC (Pakistan) for financial support. C.W would like to thank EPSRC Integrated Photonics and Electronics Systems funding.

References

[1] B.C. O'Regan, M. Grätzel, A low-cost, high-efficiency solar cell based on dye-sensitized colloidal TiO2 films, Nature 353 (1991) 737–740, doi:http://dx.doi.org/10.1038/353737a0.
[2] S. Mathew, A. Yella, P. Gao, R. Humphry-Baker, B.F.E. Curchod, N. Ashari-Astani, et al., Dye-sensitized solar cells with 13% efficiency achieved through the molecular engineering of porphyrin sensitizers, Nat. Chem. 6 (2014) 242–247, doi:http://dx.doi.org/10.1038/nchem.1861.
[3] F. Bella, A. Sacco, D. Pugliese, M. Laurenti, S. Bianco, Additives and salts for dye-sensitized solar cells electrolytes: What is the best choice? J. Power Sources 264 (2014) 333–343, doi:http://dx.doi.org/10.1016/j.jpowsour.2014.04.088.
[4] T. Stergiopoulos, E. Rozi, C. Karagianni, P. Falaras, Influence of electrolyte co-additives on the performance of dye-sensitized solar cells, Nanoscale Res. Lett. 6 (2011) 307, doi:http://dx.doi.org/10.1186/1556-276X-6-307.
[5] B.E. Stathatos, P. Lianos, A.S. Vuk, B. Orel, Optimization of a Quasi-Solid-State Dye-Sensitized Photoelectrochemical Solar Cell Employing a Ureasil/Sulfolane Gel Electrolyte, Adv. Funct. Mater. 14 (2004) 45–48, doi:http://dx.doi.org/10.1002/adfm.200304479.
[6] V. Jovanovski, B. Orel, R. Ješe, A.Š. Vuk, G. Mali, S.B. Hočevar, et al., Novel polysilsesquioxane – I-/I3- ionic electrolyte for dye-sensitized photoelectrochemical cells, J. Phys. Chem. B 109 (2005) 14387–14395, doi:http://dx.doi.org/10.1021/jp051270c.
[7] T.M. Koh, H. Li, K. Nonomura, N. Mathews, A. Hagfeldt, M. Grätzel, et al., Photovoltage enhancement from cyanobiphenyl liquid crystals and 4-tert-butylpyridine in Co(II/III) mediated dye-sensitized solar cells, Chem. Commun. (Camb) 49 (2013) 9101–9103, doi:http://dx.doi.org/10.1039/c3cc43892a.
[8] S.K. Ahn, T. Ban, P. Sakthivel, J.W. Lee, Y.S. Gal, J.K. Lee, et al., Development of dye-sensitized solar cells composed of liquid crystal embedded, electrospun poly(vinylidene fluoride-co-hexafluoropropylene) nanofibers as polymer gel electrolytes, ACS Appl, Mater. Interfaces. 4 (2012) 2096–2100, doi:http://dx.doi.org/10.1021/am3000598.
[9] Sivaramakrishna Chandrasekhar, Liquid Crystals, Cambridge University Press, 1992.
[10] A. Fechtenko, K. Mu, E. Moons, R.H. Friend, J.D. Mackenzie, Self-Organized Discotic Liquid Crystals for High-Ef ciency Organic Photovoltaics, Science (80-.) 293 (2001) 1119–1122, doi:http://dx.doi.org/10.1126/science.293.5532.1119.
[11] M. Carrasco-Orozco, W.C. Tsoi, M. O'Neill, M.P. Aldred, P. Vlachos, S.M. Kelly, New photovoltaic concept: Liquid-crystal solar cells using a nematic gel template, Adv. Mater. 18 (2006) 1754–1758, doi:http://dx.doi.org/10.1002/adma.200502008.
[12] K. Sun, Z. Xiao, S. Lu, W. Zajaczkowski, W. Pisula, E. Hanssen, et al., A molecular nematic liquid crystalline material for high-performance organic photovoltaics, Nat. Commun. 6 (2015) 6013, doi:http://dx.doi.org/10.1038/ncomms7013.
[13] M.P. Aldred, A.E.A. Contoret, S.R. Farrar, S.M. Kelly, D. Mathieson, M. O'Neill, et al., A full-color electroluminescent device and patterned photoalignment using light-emitting liquid crystals, Adv. Mater. 17 (2005) 1368–1372, doi:http://dx.doi.org/10.1002/adma.200500258.
[14] S.G. Kim, S.M. Kim, Y.S. Kim, H.K. Lee, S.H. Lee, G.D. Lee, et al., Stabilization of the liquid crystal director in the patterned vertical alignment mode through formation of pretilt angle by reactive mesogen, Appl. Phys. Lett. 90 (2007) 3–6, doi:http://dx.doi.org/10.1063/1.2752105.
[15] M. Law, L.E. Greene, J.C. Johnson, R. Saykally, P.D. Yang, Nanowire dye-sensitized solar cells, Nat. Mater. 4 (2005) 455–459, doi:http://dx.doi.org/10.1038/nmat1387.
[16] B. Liu, E.S. Aydil, Growth of oriented single-crystalline rutile TiO 2 nanorods on transparent conducting substrates for dye-sensitized solar cells, J. Am. Chem. Soc. 131 (2009) 3985–3990, doi:http://dx.doi.org/10.1021/ja8078972.
[17] J.Y. Lim, C.S. Lee, J.M. Lee, J. Ahn, H.H. Cho, J.H. Kim, Amphiphilic block-graft copolymer templates for organized mesoporous TiO2 films in dye-sensitized solar cells, J. Power Sources 301 (2016) 18–28, doi:http://dx.doi.org/10.1016/j.jpowsour.2015.09.109.
[18] D. Högberg, B. Soberats, S. Uchida, M. Yoshio, L. Kloo, H. Segawa, et al., Nanostructured Two-Component Liquid-Crystalline Electrolytes for High-Temperature Dye-Sensitized Solar Cells, Chem. Mater. (2014) 26, doi:http://dx.doi.org/10.1021/cm503090z.
[19] H. Shirakawa, K. Akagi, S. Katayama, K. Araya, A. Mukoh, T. Narahara, Synthesis, Characterization, and Properties of Aligned Polyacetylene Films, J. Macromol. Sci. Part A Chem. 25 (1988) 643–654, doi:http://dx.doi.org/10.1080/00222338808053390.
[20] K. Watanabe, K. Suda, K. Akagi, Hierarchically self-assembled helical aromatic conjugated polymers, J. Mater. Chem. C 1 (2013) 2797, doi:http://dx.doi.org/10.1039/c3tc00045a.
[21] S.-W. Kang, S.-H. Jin, L.-C. Chien, S. Sprunt, Spatial and Orientational Templating of Semiconducting Polymers in a Cholesteric Liquid Crystal, Adv. Funct. Mater 14 (2004) 329–334, doi:http://dx.doi.org/10.1002/adfm.200305083.
[22] J. Newton, H. Coles, P. Hodgeb, J. Hannington, Synthesis and Properties of Low-molar-mass Liquid-crystalline Siloxane Derivatives, J. Mater. Chem. 4 (1994) 869–874, doi:http://dx.doi.org/10.1039/jm9940400869.
[23] N. Kapernaum, F. Knecht, C.S. Hartley, J.C. Roberts, R.P. Lemieux, F. Giesselmann, Formation of smectic phases in binary liquid crystal mixtures with a huge length ratio, Beilstein, J. Org. Chem. 8 (2012) 1118–1125, doi:http://dx.doi.org/10.3762/bjoc.8.124.
[24] M. Zistler, P. Wachter, P. Wasserscheid, D. Gerhard, A. Hinsch, R. Sastrawan, et al., Comparison of electrochemical methods for triiodide diffusion coefficient measurements and observation of non-Stokesian diffusion behaviour in binary mixtures of two ionic liquids, Electrochim. Acta 52 (2006) 161–169, doi:http://dx.doi.org/10.1016/j.electacta.2006.04.050.

[25] Z. Xue, D. He, X. Xie, Poly(ethylene oxide)-based electrolytes for lithium-ion batteries, J. Mater. Chem. A 3 (2015) 19218–19253, doi:http://dx.doi.org/10.1039/C5TA03471J.
[26] P.W. Majewski, M. Gopinadhan, W.S. Jang, J.L. Lutkenhaus, C.O. Osuji, Anisotropic ionic conductivity in block copolymer membranes by magnetic field alignment, J. Am. Chem. Soc. 132 (2010) 17516–17522, doi:http://dx.doi.org/10.1021/ja107309p.
[27] H. Maekawa, R. Tanaka, T. Sato, Y. Fujimaki, T. Yamamura, Size-dependent ionic conductivity observed for ordered mesoporous alumina-LiI composite, Solid State Ionics 175 (2004) 281–285, doi:http://dx.doi.org/10.1016/j.ssi.2003.12.032.
[28] F.E. Gálvez, P.R.F. Barnes, J. Halme, H. Míguez, Dye sensitized solar cells as optically random photovoltaic media, Energy Environ. Sci. 7 (2014) 689, doi:http://dx.doi.org/10.1039/c3ee42587h.
[29] J. Franklin, Z.Y. Wang, Refractive index matching: A general method for enhancing the optical clarity of a hydrogel matrix, Chem. Mater. 14 (2002) 4487–4489, doi:http://dx.doi.org/10.1021/cm025541x.
[30] W. Kwon, Y.-J. Chang, Y.-C. Park, H.M. Jang, S.-W. Rhee, A light scattering polymer gel electrolyte for high performance dye-sensitized solar cells, J. Mater. Chem. 22 (2012) 6027, doi:http://dx.doi.org/10.1039/c2jm15889b.
[31] K. Zhu, N.R. Neale, A. Miedaner, A.J. Frank, Enhanced charge-collection efficiencies and light scattering in dye-sensitized solar cells using oriented TiO2 nanotubes arrays, Nano Lett. 7 (2007) 69–74, doi:http://dx.doi.org/10.1021/nl062000o.
[32] R. Komiya, L. Han, R. Yamanaka, A. Islam, T. Mitate, Highly efficient quasi-solid state dye-sensitized solar cell with ion conducting polymer electrolyte, J. Photochem. Photobiol. A Chem. 164 (2004) 123–127, doi:http://dx.doi.org/10.1016/j.jphotochem.2003.11.015.
[33] Y.P. Que, J. Weng, L.H. Hu, J.H. Wu, S.Y. Dai, High open voltage and superior light-harvesting dye-sensitized solar cells fabricated by flower-like hierarchical TiO2 composed with highly crystalline nanosheets, J. Power Sources 307 (2016) 138–145, doi:http://dx.doi.org/10.1016/j.jpowsour.2015.12.061.
[34] C. Zhang, Y. Xie, T. Bai, J. Hu, J. Wang, Cooperation of multifunction composite structures and fluorescein for photovoltaic performance-enhanced ZnO-based dye-sensitized solar cells, J. Power Sources 297 (2015) 16–22, doi:http://dx.doi.org/10.1016/j.jpowsour.2015.07.092.
[35] W. Yang, Y. Hao, P. Ghamgosar, G. Boschloo, hermal Stability Study of Dye-Sensitized Solar Cells with Cobalt Bipyridyl–based Electrolytes, Electrochem. Acta 213 (2016) 879–886, doi:http://dx.doi.org/10.1016/j.electacta.2016.07.112 Submitt. under Rev.
[36] S. Ahmed, A. Du Pasquier, T. Asefa, D.P. Birnie, Improving microstructured TiO 2 photoanodes for dye sensitized solar cells by simple surface treatment, Adv. Energy Mater. 1 (2011) 879–887, doi:http://dx.doi.org/10.1002/aenm.201100121.
[37] J. Xu, S. Wu, J.H. Ri, J. Jin, T. Peng, Bilayer film electrode of brookite TiO2 particles with different morphology to improve the performance of pure brookite-based dye-sensitized solar cells, J. Power Sources 327 (2016) 77–85, doi:http://dx.doi.org/10.1016/j.jpowsour.2016.07.017.
[38] R. Kern, R. Sastrawan, J. Ferber, R. Stangl, J. Luther, Modeling and interpretation of electrical impedance spectra of dye solar cells operated under open-circuit conditions, Electrochim. Acta 47 (2002) 4213–4225, doi:http://dx.doi.org/10.1016/S0013-4686(02)00444-9.
[39] A. Burke, S. Ito, H. Snaith, U. Bach, J. Kwiatkowski, M. Grätzel, The function of a TiO2 compact layer in dye-sensitized solar cells incorporating planar organic dyes, Nano Lett. 8 (2008) 977–981, doi:http://dx.doi.org/10.1021/nl071588b.